ELSEVIER

Earth and Planetary Science Letters 159 (1998) 25–33

EPSL

Brillouin scattering and X-ray diffraction of San Carlos olivine: direct pressure determination to 32 GPa

Chang-sheng Zha [a], Thomas S. Duffy [b,*], Robert T. Downs [c], Ho-kwang Mao [a], Russell J. Hemley [a]

[a] *Geophysical Laboratory and Center for High-Pressure Research, Carnegie Institution of Washington, 5251 Broad Branch Road NW, Washington, DC 20015, USA*

[b] *Department of Geosciences, Princeton University, Princeton, NJ 08544, USA*

[c] *Department of Geological Sciences, University of Arizona, Tucson, AZ 85721, USA*

Received 6 June 1997; accepted 26 March 1998

Abstract

The single-crystal elastic moduli of San Carlos olivine, $(Mg_{0.9}Fe_{0.1})_2SiO_4$, were determined at seven pressures between 2.5 and 32.5 GPa by Brillouin spectroscopy in a diamond anvil cell. The unit cell volume was also determined at each pressure (and ambient pressure) by single-crystal X-ray diffraction. The shear elastic moduli exhibit non-linear pressure dependencies. In particular, a non-linear dependence is required for the elastic modulus, C_{55}, above 10 GPa. Aggregate bulk and shear moduli were determined from Hashin–Shtrikman averages of the individual constants. Pressures were determined by fitting the bulk modulus (Reuss bound) and volume data to a third-order Eulerian finite strain equation and integrating. The results are compared to independent pressure measurements made using the ruby fluorescence scale. The ruby measurements yield pressures that are in good agreement with the Brillouin results. On average, the ruby fluorescence measurements produce pressures that are larger than the Brillouin determinations by 1.6%.

Keywords: elasticity; olivine; high pressure; upper mantle

1. Introduction

Development of an accurate pressure scale is central to high-pressure science and technology. The ruby fluorescence technique provides a convenient and precise secondary pressure scale and its development was one of the major factors leading to the widespread use of the diamond anvil cell [1–3]. Initially, the pressure-induced fluorescence wavelength shift of ruby was calibrated against X-ray diffraction data for NaCl to 20 GPa [2] using the semi-empirical Decker equation of state [4] which has an accuracy of about 3%. Subsequently, the ruby scale was extended to pressures above 100 GPa by calibration of the wavelength shift against isotherms derived from shock-compression of several metals [3]. Again, the systematic uncertainty for this curve is estimated to be about 3%. A slightly different calibration for materials subjected to quasi-hydrostatic compression through the use of soft solid pressure media has also been developed [5]. Recently, new techniques to ex-

* Corresponding author. Tel.: +1 (609) 258-6769; Fax: +1 (609) 258-1274; E-mail: duffy@geo.princeton.edu

0012-821X/98/$19.00
PII S0012-821X(98)00063-6

cite strong ruby fluorescence at pressures as high as 251 GPa have been explored [6].

While a major advantage of the ruby scale is its high precision, it has long been recognized that the accuracy of this scale is limited. Above 10 GPa, the pressure calibration is determined by dynamic compression data.

This suffers from uncertainties due to: (1) the experimental precision of the Hugoniot and static compression measurements; (2) neglect of contributions due to static and dynamic shear strengths; and (3) thermal correction from Hugoniot states to the static isotherm. Since the initial measurements calibrating the scale to 100 GPa [3], experiments have demonstrated that metals can support significant shear stresses under both dynamic and static high pressures [7–9].

It was first pointed out more than 40 years ago that precise measurements of sound velocity and volume, together with some thermodynamic parameters are sufficient for direct determination of pressure in a high-pressure device [10]. However, the lack of high-pressure elasticity data has limited use of this method to very low pressures [11]. In this study, we derive a direct pressure scale, accurate to ±2%, based on elasticity and diffraction data for San Carlos olivine to 32 GPa.

The elastic properties of olivines at high pressure and temperature are central to the interpretation of seismic data for the Earth's upper mantle [12]. In the $(Mg, Fe)_2SiO_4$ system, numerous high-pressure experimental and theoretical studies of the crystal structure at high pressure have been reported [13–16]. There have also recently been several measurements of elastic properties to pressures as high as 17 GPa [17–23]. Changes in the compression mechanism of Mg_2SiO_4 have been proposed based on X-ray diffraction and spectroscopic data at 9 GPa [24], 17 GPa [13], and 42 GPa [14]. However, no structural discontinuity was observed during compression of forsterite to 17.2 GPa using helium as a quasi-hydrostatic medium [15].

When compressed at room temperature, olivines remain stable at pressures well above their thermodynamic stability but progressively transform to an amorphous phase [14]. There is little direct information on how the elastic moduli of a material behave when it is compressed far outside its stability field and approaches the region of pressure-induced amorphization. It has been proposed that lattice instabilities are the driving force behind this form of solid state amorphization [25,26]. According to the model of the latter study, the amorphization process is controlled by the competition between stabilizing noncentral covalent forces and destabilizing nearest-neighbor repulsion. A softening of the elastic constants is predicted as the structural instability is approached. There are currently very few measurements of elastic moduli in the metastable or amorphous regime to test the predictions of this theory.

2. Experimental method

The composition of the gem-quality natural samples of San Carlos olivine was determined by electron microprobe analysis to be $(Mg_{0.9}Fe_{0.1})_2SiO_4$. Samples were polished on both sides in a plane that intersects the three crystal axes at nearly equal angles. A 60-μm thick piece was loaded into a diamond anvil cell together with an argon pressure medium and Brillouin spectra were recorded at 2.5 and 5.0 GPa. The same crystal was then reloaded with a methanol–ethanol medium and spectra were recorded at 8.6 GPa. Upon increasing pressure to 10.3 GPa, the sample broke apart and no spectra were obtained at this pressure. A 10-μm thick sample was then loaded with a helium pressure medium. Brillouin spectra were recorded between 14 and 32 GPa with this sample. Pressures were determined by ruby fluorescence. There were slight differences (∼0.2 GPa) between the pressure determinations made during the X-ray diffraction experiments and during the Brillouin measurements.

In Brillouin scattering, acoustic velocities are determined from the Doppler-shifted frequency of scattered laser light. Single-frequency radiation at 514.5 nm and a 90° scattering geometry were used. The scattered light was collected, spatially filtered, and passed through a Sandercock-type tandem vernier 3 + 3 Fabry–Perot interferometer. The signal was detected by a photomultiplier tube using photon-counting electronics and the spectrum was recorded with a multi-channel scaler. Details of the Brillouin scattering system are contained in Ref. [20].

At each pressure, the orientation and lattice constants were computed from the positions of 6–10 accessible peaks in the 11–25° 2θ range that were measured using single-crystal X-ray diffraction on a Picker four-circle diffractometer with Mo Kα radiation using. The cell volumes were computed by constraining all unit cell angles to be 90°. Only slight differences in the volumes result when the angles are unconstrained. This signifies that the crystal is not being subjected to significant shear strain. The datum at 32 GPa was collected using the Laue energy-dispersive technique with synchrotron radiation (National Synchrotron Light Source, beamline X17C) [27]. The cell constants were obtained using 25 peaks in the d-spacing range to 1.12 Å. In addition to the high-pressure measurements, the ambient-pressure cell volume was measured to be 292.0 (1) $Å^3$, where the number in parentheses is the 2σ uncertainty. This value is in good agreement with the expected value calculated from end-member properties [28]. Further details of the X-ray experiments are provided elsewhere [15].

3. Results

The results of the X-ray diffraction experiments are shown in Table 1 and plotted in Fig. 1 using the quasi-hydrostatic ruby fluorescence pressure scale [5]. The volume compression data are in good agreement with earlier results for San Carlos olivine [23] and forsterite [15]. The number and quality of X-ray diffraction peaks obtained for the datum at a ruby fluorescence pressure of 8.6 GPa were significantly reduced compared with the remainder of the data. In the past, such deteriorations in X-ray data quality have been associated with samples experiencing a significant degree of non-hydrostatic stress [15]. As a consequence, this datum was not included in any of the subsequent analysis. Fitting the remaining seven data points to a third-order Birch–Murnaghan equation yields a bulk modulus of 129.9 (0.6) GPa when the pressure derivative is fixed at 4.0.

At each pressure, the compressional and two shear acoustic velocities were determined by Brillouin scattering for approximately 18 directions at 10° intervals within the plane perpendicular to the diamond cell axis. The elasticity and orientation data were jointly inverted using non-linear least squares to obtain the nine independent elastic moduli and three angles which describe the crystal orientation. Starting values for the orientation were taken from X-ray data and final values agreed with starting values within mutual uncertainties. For the elastic moduli, starting values were generally taken from measurements at the preceding pressure, but a wider range of starting models were also tested. The root-mean-square deviations between calculated and measured velocities ranged from 3 m/s to 48 m/s, and were generally larger at higher pressures, due to the smaller sample size above 14 GPa.

The pressure dependencies of the nine independent elastic moduli are shown in Fig. 2 and Table 2. Uncertainties (2σ) in the longitudinal moduli (C_{11}, C_{22}, C_{33}) are typically 3–4%, in the shear moduli (C_{44}, C_{55}, C_{66}) 2–3%, and in the off-diagonal moduli (C_{12}, C_{13}, C_{23}) 5–10%. The longitudinal moduli (C_{11}, C_{22}, and C_{33}) are generally consistent with the results of earlier studies to 12 GPa. In general, small but non-negligible quadratic terms are required to

Table 1
X-ray diffraction data for San Carlos olivine

P (GPa)	a (Å)	b (Å)	c (Å)	V ($Å^3$)	Density (g/cm^3)
0.0	4.7631 (14)	10.2272 (9)	5.9944 (10)	292.01 (10)	3.343 (1)
2.5	4.7415 (13)	10.1458 (17)	5.9589 (13)	286.67 (9)	3.406 (1)
5.0	4.724 (3)	10.065 (4)	5.925 (2)	281.7 (2)	3.466 (2)
8.6	4.738 (13)	9.917 (13)	5.874 (16)	276.0 (9)	3.537 (12)
14.2	4.6651 (9)	9.825 (2)	5.811 (1)	266.34 (7)	3.666 (1)
19.6	4.637 (2)	9.715 (3)	5.765 (2)	259.7 (1)	3.759 (1)
25.6	4.613 (1)	9.593 (2)	5.708 (1)	252.58 (8)	3.865 (1)
32.4	4.575 (2)	9.456 (4)	5.646 (2)	244.2 (1)	3.998 (2)

Pressures are from ruby fluorescence. Uncertainties are 1 standard deviation.

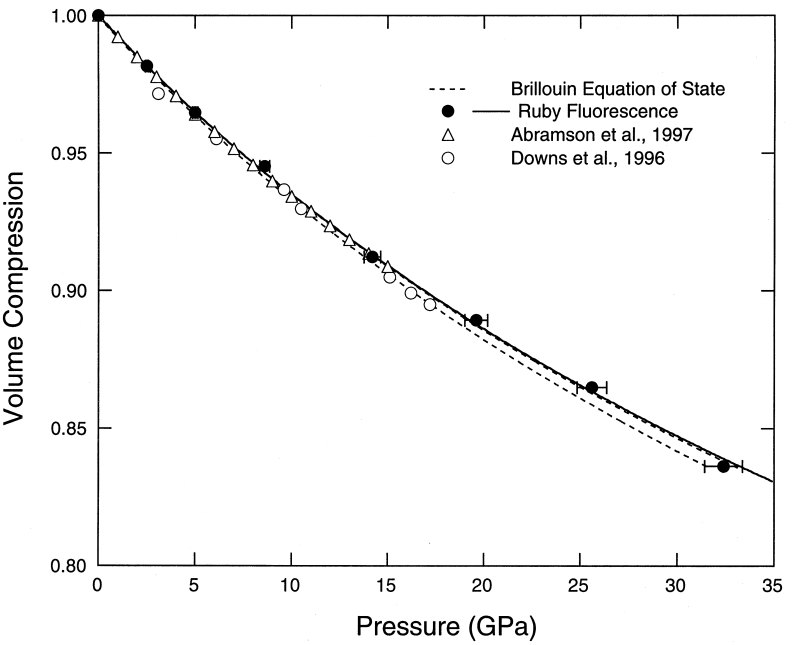

Fig. 1. Volume compression data for San Carlos olivine. Filled symbols are X-ray volume determinations with ruby fluorescence pressure measurements (with ±3% uncertainty). The solid line is a third-order finite strain fit to these data. The dashed lines show the upper and lower limits of the pressure determined from Brillouin/diffraction data as discussed in the text. The upper limit of Brillouin data nearly overlaps the finite strain fit from ruby fluorescence data. Also shown are previous data for San Carlos olivine [23] and forsterite [15] based on the ruby pressure scale.

Table 2
Single-crystal elastic moduli of San Carlos olivine

P	C_{11}	C_{22}	C_{33}	C_{44}	C_{55}	C_{66}	C_{12}	C_{13}	C_{23}
2.5	332.5 (10.8)	209.4 (6.8)	251.4 (8.2)	68.7 (1.7)	80.1 (2.1)	82.7 (1.9)	80.7 (7.4)	80.2 (6.8)	84.4 (5.0)
5.0	352.8 (11.4)	224.2 (7.2)	267.1 (8.2)	70.8 (1.6)	85.7 (2.3)	90.2 (2.2)	91.2 (7.6)	92.7 (7.4)	95.2 (5.2)
8.1	378.9 (11.6)	244.0 (8.2)	283.5 (9.0)	77.6 (2.0)	91.9 (1.9)	96.3 (2.7)	100.8 (8.6)	102.3 (7.8)	104.7 (6.0)
14.1	395.3 (11.6)	270.4 (13.0)	295.3 (8.8)	81.2 (1.6)	96.6 (1.8)	103.6 (3.5)	122.5 (10.0)	118.0 (7.6)	123.0 (9.2)
18.8	424.1 (12.6)	270.4 (12.6)	326.8 (9.8)	86.3 (2.2)	99.8 (2.0)	112.8 (2.9)	129.2 (13.4)	133.2 (8.2)	138.2 (8.8)
24.6	442.2 (12.0)	292.0 (13.2)	339.8 (10.0)	87.6 (2.1)	102.5 (1.7)	118.4 (3.1)	138.8 (13.0)	148.7 (8.2)	161.7 (8.2)
32.3	481.4 (12.8)	311.6 (12.8)	386.7 (10.6)	89.7 (2.2)	106.2 (2.0)	123.2 (3.3)	166.8 (12.6)	185.8 (8.6)	185.3 (9.0)

All values in GPa. Uncertainties are 2 standard deviations. Pressures are from integration of Brillouin and X-ray data as discussed in the text.

explain the pressure dependence of the elastic moduli in San Carlos olivine to 32 GPa. The non-linear pressure dependence of the shear moduli (C_{44}, C_{55}, C_{66}) is stronger than that of the longitudinal moduli, although a significant non-linearity is also observed in C_{22} above 14 GPa.

There is generally good agreement between the present results and previous data to 17 GPa reported using the impulsive stimulated scattering (ISS) technique [23]. Interpolated values for C_{11} and C_{33} are 4.9% and 4.0% lower than measurements at 17 GPa reported in Ref. [23]. A stronger non-linear pressure dependence is also observed here for C_{44} compared with that found in Ref. [23].

There has been some controversy regarding the behavior of the modulus C_{55} in San Carlos olivine. Initial studies based on the ISS technique [19] showed a strong non-linearity in C_{55} that was not

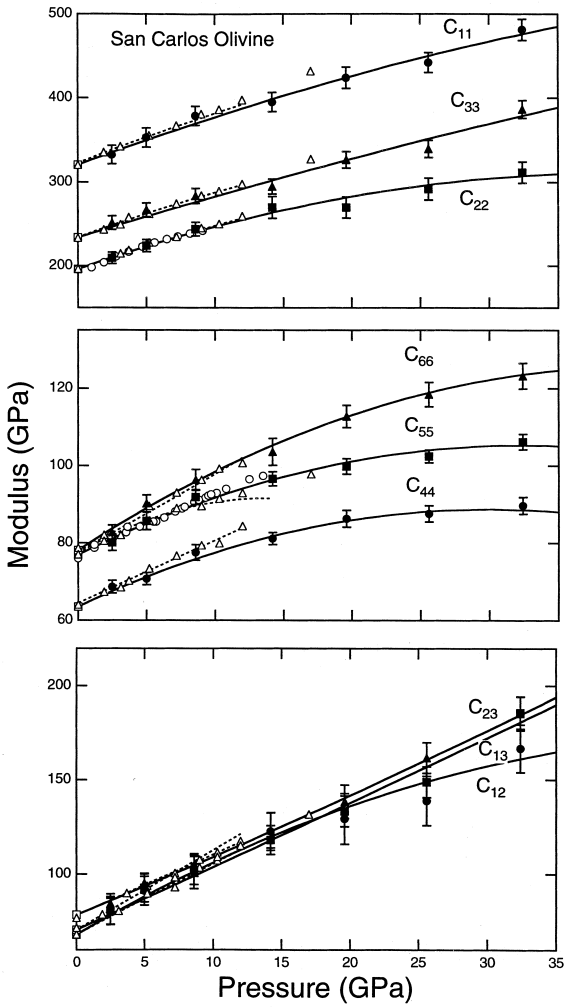

Fig. 2. Single-crystal elastic moduli of San Carlos olivine as a function of pressure. Filled symbols, present data with 2σ uncertainties; squares, [17]; circles, [22]; triangles, [23]; dashed line, [19]. The solid lines are weighted least squares fits to the present data and the ambient-pressure data of Ref. [17]. Pressures were determined by ruby fluorescence, and fitting curves change only slightly when pressures from Brillouin data (discussed below) are used.

observed in later ultrasonic multi-anvil experiments to 13 GPa [22]. In more recent ISS results to 17 GPa, the non-linearity in C_{55} is reduced but still present [23]. Within uncertainties, the present results are in agreement with both the most recent ISS data [23] and the ultrasonic data [22]. However, extension of the data set to 32 GPa clearly shows that a non-linear term is required to describe the pressure dependence C_{55} in San Carlos olivine. A weighted least squares fit to the present data yields: $C_{55} = 77.7(2.2) + 1.65(0.31)P - 0.025(009)P^2$, where P is the pressure in GPa.

Single-crystal elasticity data for forsterite to 16 GPa require no such non-linearity in C_{55} or the other shear moduli (C_{44}, C_{66}) [20]. The behavior of the shear elastic moduli in olivine may be strongly sensitive to Fe content. In a recent non-hydrostatic X-ray diffraction study, the pressure at which the olivine compression regime was observed to change is strongly dependent on Fe content, varying from 42 GPa in forsterite to 10 GPa in fayalite [14]. Similarly, the range of pressures over which amorphization occurs is higher for Mg-rich olivines than for Fe-rich olivines [14]. It is possible that the non-linearity of the shear constants in San Carlos olivine reflects the beginnings of a lattice instability that ultimately leads to pressure-induced amorphization as the material is compressed outside its thermodynamic stability field [25,26]. If this hypothesis is true, one might expect to detect non-linearities in the shear constants of forsterite at higher pressures, and presumably, in fayalite or more Fe-rich olivines at lower pressures.

Aggregate bulk and shear moduli were calculated from the single-crystal stiffnesses using the variational method of Hashin and Shtrikman [29] (Fig. 3; Table 3). The separation of the upper and lower bounds in San Carlos olivine is very small (a few tenths of a per cent). The major contributor to the uncertainty in the Hashin–Shtrikman average is the uncertainty in the bounds themselves. The data were fit to third- and fourth-order Eulerian finite strain expressions using non-linear least squares. The results of the fits are listed in Table 4.

Ambient-pressure moduli were included in the fit, and values were taken from the mean of seven reported values of the moduli of San Carlos with Fe mole fractions ranging from 0.07 to 0.10. The resulting averages are: $K_{0S} = 129.1$ (2.8) and $G_0 = 78.5$ (1.2), where K_{0S} and G_0 are the ambient-pressure adiabatic bulk and shear moduli, respectively, and the numbers in parentheses are 2 standard deviation uncertainties.

For the bulk modulus, the third- and fourth-order finite strain expressions yield similar curves which fit the data nearly equally well (Fig. 3). However,

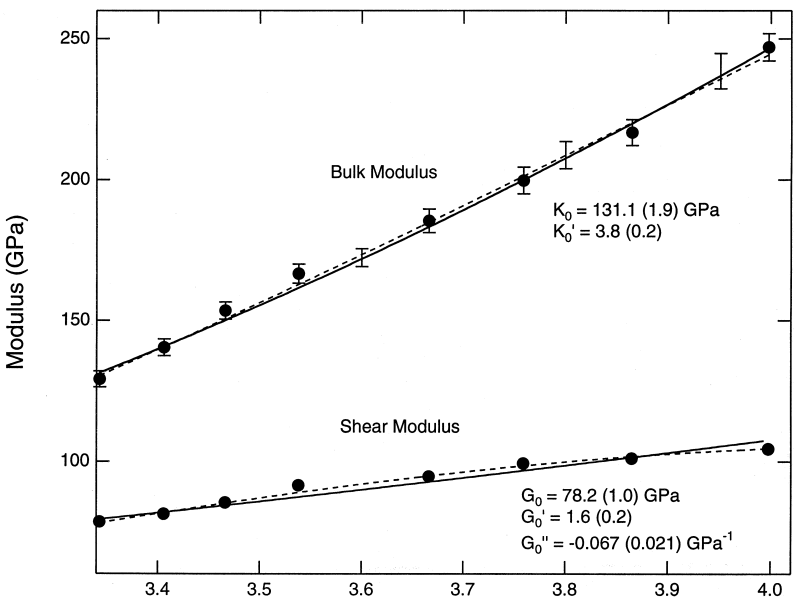

Fig. 3. Aggregate bulk (K_S) and shear (G) moduli of San Carlos olivine as a function of pressure. Symbols are Hashin–Shtrikman averages. The uncertainties are approximately the symbol size for the shear modulus. Solid and dashed lines are third- and fourth-order finite strain fits to the data. Ambient-pressure value is the mean of results from seven published studies. Error bars on solid curve show 2σ uncertainties on the third-order finite strain fit for the bulk modulus.

Table 3
Aggregate elastic properties of San Carlos olivine

P (GPa)	K_S (GPa)	G (GPa)	V_P (km/s)	V_B (km/s)	V_S (km/s)	σ
2.5	140.5 (3.0)	81.4 (1.4)	8.55 (0.06)	6.42 (0.07)	4.89 (0.04)	0.257 (0.008)
5.0	153.5 (3.1)	85.5 (1.4)	8.79 (0.06)	6.65 (0.07)	4.97 (0.04)	0.265 (0.007)
8.1	166.7 (3.4)	91.6 (1.6)	9.03 (0.07)	6.87 (0.07)	5.09 (0.05)	0.267 (0.009)
14.1	185.5 (4.2)	94.8 (1.9)	9.22 (0.07)	7.12 (0.08)	5.09 (0.05)	0.279 (0.008)
18.8	199.7 (4.7)	99.4 (2.1)	9.40 (0.08)	7.29 (0.09)	5.14 (0.05)	0.287 (0.008)
24.6	216.8 (4.6)	101.2 (2.1)	9.54 (0.07)	7.49 (0.08)	5.12 (0.05)	0.298 (0.007)
32.3	247.0 (4.8)	104.5 (2.2)	9.83 (0.007)	7.86 (0.008)	5.11 (0.05)	0.315 (0.006)

Bulk and shear moduli are averages of the Hashin–Shtrikman bounds. Uncertainties are 2 standard deviations. Pressures are from integration of Brillouin and X-ray data as discussed in the text.

the pressure derivatives are not well constrained in the case of the fourth-order fit (Table 4). As the pressure derivatives obtained from the two fits are not significantly different, the third-order fit is used in the subsequent analysis. For the shear modulus, it is apparent in Fig. 3 that the fourth-order equation provides a better fit to the data than the third-order equation. The first pressure derivatives from the two fits are significantly different at the 2σ level in this case. The larger non-linearity of the shear constants requires the use of the higher-order equation.

The aggregate compressional (V_P), bulk (V_B), and shear (V_S) wave velocities are listed in Table 3, together with Poisson's ratio, σ. Poisson's ratio increases strongly with pressure from an ambient-pressure value of 0.24 to 0.32 at 32 GPa.

4. Discussion

Measurements of sound velocity and volume, together with values for some thermodynamic parame-

Table 4
Fit parameters for Eulerian finite strain equations

	K_{0S} (GPa)	K'_{0S}	K''_{0S} (GPa^{-1})	G_0 (GPa)	G'_0	G''_0 (GPa^{-1})
3rd order	131.1 (1.9)	3.8 (0.2)	–	79.4 (0.8)	1.0 (0.1)	–
4th order	130.0 (2.2)	4.2 (0.6)	−0.074 (0.066)	78.2 (1.0)	1.6 (0.2)	−0.067 (0.021)

The numbers in parentheses are 2 standard deviation uncertainties. K_{0S}, G_0 are the mean Hashin–Shtrikman bounds on the ambient-pressure adiabatic bulk modulus and shear modulus. Single and double primes represent first and second pressure derivatives of the moduli, respectively.

ters are sufficient for direct determination of pressure in a high-pressure device through the thermodynamic relation [11]:

$$K_T = -V\left(\frac{\partial P}{\partial V}\right)_T = K_S/(1+\alpha\gamma T) \quad (1)$$

where K_T and K_S are the isothermal and adiabatic incompressibilities, respectively, α is the volume coefficient of thermal expansivity, γ is the Gruneisen parameter, and P, V, T are pressure, volume, and temperature, resp.

Integration yields:

$$P = P_0 - \int_{V_0}^{V} \frac{K_T dV}{V} = P_0 - \int_{V_0}^{V} \frac{K_S dV}{V(1+\alpha\gamma T)} \quad (2)$$

The third-order Eulerian finite strain expression for the bulk modulus is given by:

$$K = (1+2f)^{5/2} K_0 \left[1 + (3K'_0 - 5) f\right] \quad (3)$$

where K_0 and $K'_0 = (\partial K_0/\partial P)_T$ can represent either the isothermal or adiabatic bulk modulus and its pressure derivative. The Eulerian strain, f, is given by:

$$f = \tfrac{1}{2}\left[\left(\frac{V_0}{V}\right)^{2/3} - 1\right] \quad (4)$$

where V is the volume.

Inserting Eq. 3 into Eq. 2 and integrating yields the familiar Birch–Murnaghan expression for the pressure:

$$P = 3K_{0T} f (1+2f)^{5/2}\left[1 + \tfrac{3}{2}\left(K'_{0T} - 4\right) f\right] \quad (5)$$

To compute pressures from the X-ray and Brillouin data appropriate for comparison with ruby fluorescence data, we first computed the Reuss (constant stress) bound on the adiabatic bulk modulus, K_S^R, at each pressure. Fitting the X-ray volumes and K_S^R to a third-order finite strain equation of state yielded a value of 129.3 (1.9) for the Reuss bound on the ambient-pressure adiabatic bulk modulus, K_{0S}^R, and a value of 3.8 (0.2) for the pressure derivative, $(\partial K_{0S}^R/\partial P)_T$.

The ambient-pressure modulus and pressure derivative were then corrected from adiabatic to isothermal conditions using Eq. 1 and:

$$\left(\frac{\partial K_{0S}}{\partial P}\right)_T \approx \left(\frac{\partial K_{0T}}{\partial P}\right)_T (1+\alpha\gamma T) + \frac{\gamma T}{K_{0T}}\left(\frac{\partial K_{0T}}{\partial T}\right)_P - \alpha\gamma T \quad (6)$$

where it has been assumed that the product of density and Gruneisen parameter is constant.

Since the thermodynamic parameters, α, γ, and $(\partial K_T/\partial T)_P$ were not directly measured, it is not possible to perform a completely self-consistent calculation. Fortunately, the necessary parameters are well-constrained for San Carlos olivine [30,31], and, as a result, the small adiabatic–isothermal corrections contribute negligibly to the overall uncertainty in the pressure determination. The resulting values for isothermal moduli are: $K_{0T}^R = 128.0\,(1.9)$ GPa and $(\partial K_{0T}^R/\partial P)_T = 3.84\,(0.20)$.

These values were then used to calculate the pressure as a function of strain using Eq. 5 (Fig. 1). The dashed lines in the figure represent upper and lower bounds on the pressure obtained by propagating uncertainties in Eq. 5. The uncertainty in the pressure determination by the Brillouin/diffraction technique is approximately ±2%. As shown in Fig. 1, the ruby fluorescence pressures are generally in good agreement with the Brillouin determinations, but tend to lie at slightly higher pressures than the Brillouin results. The fit to the ruby data (solid line, Fig. 1) produces pressures that exceed the mean Brillouin

pressure by 2.0% at 10 GPa, 2.5% at 20 GPa, and 2.9% at 30 GPa.

The isothermal bulk modulus as a function of strain was calculated using Eq. 3. Comparing the isothermal and adiabatic bulk moduli at high pressure, our results imply that $K_S/K_T = 1 + \alpha\gamma T$ decreases from 1.01 at 1 bar to 1.005 at 32 GPa.

Fig. 4 shows the difference in pressure between the ruby fluorescence and Brillouin determinations plotted as a function of the Brillouin pressure. In all cases, the pressure differences are within the combined 3% uncertainty in ruby scale and 2% uncertainty in the Brillouin pressure scale. Considering the individual ruby measurements, the average deviation from the mean Brillouin pressure is +0.3 GPa, and in percentage terms, it is +1.6%. The maximum deviation is 1.0 GPa.

This study demonstrates that direct pressure determination is feasible in the diamond anvil cell to very high pressure. There is good agreement between the ruby fluorescence measurements and the Brillouin pressure determinations to 32 GPa, with an average difference between the curves of only 0.3 GPa. The uncertainty in the pressure determination by the present technique is ±2%. This uncertainty can be reduced in the future by higher-precision bulk modulus determinations.

Acknowledgements

We thank J.M. Brown, W.A. Bassett, and an anonymous reviewer for thorough and thoughtful reviews. This research was supported by the NSF. The Center for High-Pressure Research is an NSF Science and Technology Center. ***[RO]***

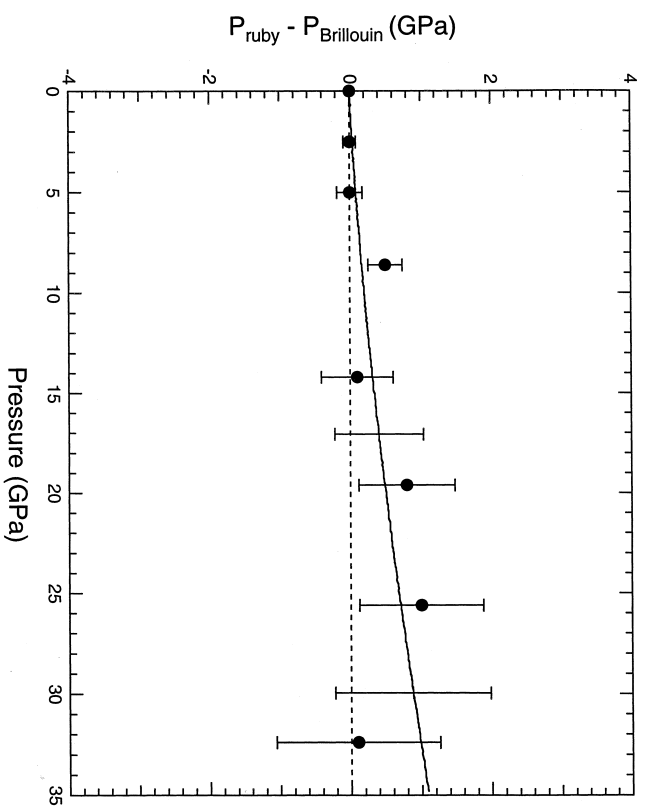

Fig. 4. Pressure difference between ruby and Brillouin pressure determinations as a function of Brillouin pressure. The solid curve is obtained from the difference between the fit to the ruby data and the mean value of the Brillouin pressure (Fig. 1). The 2σ uncertainty on this curve is shown by the error bar. The symbols show differences between individual ruby pressures measurements and pressures from Brillouin data at that density. The dashed line is a reference line at 0 GPa.

References

[1] R.A. Forman, G.J. Piermarini, J.D. Barnett, S. Block, Pressure measurement made by the utilization of ruby sharp-line luminescence, Science 176 (1972) 284–285.

[2] G.J. Piermarini, J.D. Barnett, R.A. Forman, Calibration of the pressure dependence of the R_1 ruby fluorescence line to 195 kbar, J. Appl. Phys. 46 (1975) 2774–2780.

[3] H.K. Mao, P.M. Bell, J.W. Shaner, D.J. Steinberg, Specific volume measurements of Cu, Mo, Pd, and Ag and calibration of the ruby R_1 fluorescence pressure gauge from 0.06 to 1 Mbar, J. Appl. Phys. 49 (1978) 3276–3283.

[4] D.L. Decker, High-pressure equation of state for NaCl, KCl, and CsCl, J. Appl. Phys. 42 (1971) 3239–3244.

[5] H.K. Mao, J. Xu, P.M. Bell, Calibration of the ruby pressure gauge to 800 kbar under quasi-hydrostatic conditions, J. Geophys. Res. 91 (1986) 4673–4767.

[6] N.H. Chen, I.F. Silvera, Excitation of ruby fluorescence at multimegabar pressures, Rev. Sci. Instrum. 67 (1996) 4275–4278.

[7] M.D. Furnish, L.C. Chhabildas, Dynamic properties of refractory materials: molybdenum, in: R. Asfahani, E. Chen, A. Crowson (Eds.), High Strain Rate Behavior Of refractory Metals and Alloys, The Minerals, Metal and Materials Society, Warrendale, PA, 1992, pp. 229–241.

[8] R. Jeanloz, B.K. Godwal, C. Meade, Static strength and equation of state of rhenium at ultra-high pressures, Nature 349 (1991) 687–689.

[9] R.J. Hemley, H.K. Mao, G. Shen, J. Badro, P. Gillet, M. Hanfland, D. Hausermann, X-ray imaging of stress and strain of diamond, iron, and tungsten at megabar pressures, Science 276 (1997) 1242–1245.

[10] A.H. Smith, A.W. Lawson, The velocity of sound in water as a function of temperature and pressure, J. Chem Phys. 22 (1954) 351–359.

[11] A.L. Ruoff, R.C. Lincoln, Y.C. Chen, A new method of absolute high pressure determination, J. Phys. D: Appl. Phys. 6 (1973) 1295–1306.

[12] T.S. Duffy, C.S. Zha, R.T. Downs, H.K. Mao, R.J. Hemley, Elasticity of forsterite to 16 GPa and the composition of the upper mantle, Nature 378 (1995) 170–173.

[13] Y. Kudoh, Y. Takeuchi, The crystal structure of forsterite Mg_2SiO_4 under higher pressure up to 149 kbar, Z. Kristallogr. 171 (1985) 291–302.

[14] D. Andrault, M.A. Bouhifd, J.P. Itie, P. Richet, Compression and amorphization of $(Mg,Fe)_2SiO_4$ olivines: An X-ray diffraction study up to 70 GPa, Phys. Chem. Miner. 22 (1995) 99–107.

[15] R.T. Downs, C.S. Zha, T.S. Duffy, L.W. Finger, The equation of state of forsterite to 17.2 GPa and effects of pressure media, Am. Mineral. 81 (1996) 51–55.

[16] J. Brodholt, A. Patel, K. Refson, An ab initio study of the compressional behavior of forsterite, Am. Mineral. 81 (1996) 257–260.

[17] S.L. Webb, The elasticity of the upper mantle orthosilicates olivine and garnet to 3 GPa, Phys. Chem. Mineral. 16 (1989) 684–692.

[18] A. Yoneda, M. Morioka, Pressure derivatives of elastic constants of single crystal forsterite, in: Y. Syono, M. Manghnani (Eds.), High-Pressure Research: Application to Earth and Planetary Sciences, AGU, Washington, DC, 1992, pp. 207–214.

[19] J. Zaug, E.H. Abramson, J.M. Brown, L.J. Slutsky, Sound velocities in olivine at Earth mantle pressures, Science 260 (1993) 1487–1489.

[20] C.S. Zha, T.S. Duffy, R.T. Downs, H.K. Mao, R.J. Hemley, Sound velocity and elasticity of single crystal forsterite to 16 GPa, J. Geophys. Res. 101 (1996) 17535–17545.

[21] B. Li, G.D. Gwanmesia, R.C. Liebermann, Sound velocities of olivine and beta polymorphs of Mg_2SiO_4 at Earth's transition zone pressures, Geophys. Res. Lett. 23 (1996) 2259–2262.

[22] G. Chen, B. Li, R.C. Liebermann, Selected elastic moduli of single crystal olivines from ultrasonic experiments to mantle pressures, Science 272 (1996) 979–980.

[23] E.H. Abramson, J.M. Brown, L.J. Slutsky, J. Zaug, The elastic constants of San Carlos olivine to 17 GPa, J. Geophys. Res. 102 (1997) 12253–12264.

[24] A. Chopelas, Thermal properties of forsterite at mantle pressures derived from vibrational spectroscopy, Phys. Chem. Miner. 17 (1990) 149–156.

[25] R.J. Hemley, A.P. Jephcoat, H.K. Mao, L.C. Ming, M.H. Manghnani, Pressure-induced amorphization of crystalline silica, Nature 334 (1988) 52–54.

[26] A.G. Lyapin, V.V. Brazhkin, Pressure-induced lattice instability and solid state amorphization, Phys. Rev. B 54 (1996) 12036–12048.

[27] H.K. Mao, A.P. Jephcoat, R.J. Hemley, L.W. Finger, C.S. Zha, R.M. Hazen, D.E. Cox, Synchrotron X-ray diffraction measurements of single-crystal hydrogen to 26.5 Gigapascals, Science 239 (1988) 1131–1132.

[28] J.R. Smyth, T.C. McCormick, Crystallographic data for minerals, in: T.J. Ahrens (Ed.), Mineral Physics and Crystallography: A Handbook of Physical Constants, AGU, Washington, DC, 1995, pp. 1–17.

[29] J.P. Watt, Hashin–Shtrikman bounds on the effective elastic moduli of polycrystals with orthorhombic symmetry, J. Appl. Phys. 50 (1979) 6290–6295.

[30] D.G. Isaak, High-temperature elasticity of iron-bearing olivines, J. Geophys. Res. 97 (1992) 1871–1885.

[31] O.L. Anderson, D.G. Isaak, Elastic constants of mantle minerals at high temperature, in: T.J. Ahrens (Ed.), Mineral Physics and Crystallography: A Handbook of Physical Constants, AGU, Washington, DC, 1995, pp. 64–97.